The bacterial virulence factors VopL and VopF nucleate actin from the pointed end

Thomas A. Burke,[1] Alyssa J. Harker,[1] Roberto Dominguez,[3] and David R. Kovar[1,2]

[1]Department of Molecular Genetics and Cell Biology and [2]Department of Biochemistry and Molecular Biology, The University of Chicago, Chicago, IL 60637
[3]Department of Physiology, Perelman School of Medicine, University of Pennsylvania, Philadelphia, PA 19104

VopL and VopF (VopL/F) are tandem WH2-domain actin assembly factors used by infectious *Vibrio* species to induce actin assembly in host cells. There is disagreement about the filament assembly mechanism of VopL/F, including whether they associate with the filament barbed or pointed end. Here, we used multicolor total internal reflection fluorescence microscopy to directly observe actin assembly with fluorescently labeled VopL/F. In actin monomer assembly reactions, VopL/F exclusively nucleate actin filament assemblies, remaining only briefly associated with the pointed end. VopL/F do not associate with the ends of preassembled filaments. In assembly reactions with saturating profilin, ~85% of VopL/F molecules also promote nucleation from the pointed end, whereas a smaller fraction (<15%) associate for ~25 s with the barbed end of preassembled filaments, inhibiting their elongation. We conclude that VopL/F function primarily as actin nucleation factors that remain briefly (~100 s) associated with the pointed end.

Introduction

Diverse actin filament networks are assembled, maintained, and disassembled by different sets of actin-binding proteins with complementary biochemical activities (Blanchoin et al., 2014). These networks are initiated by actin assembly factors that enhance the transition from monomeric to F-actin by catalyzing nucleation, elongation, or both. Better understood are the actin assembly mechanisms of Arp2/3 complex and formins (Chhabra and Higgs, 2007; Pollard, 2007; Chesarone and Goode, 2009; Campellone and Welch, 2010). Arp2/3 complex associates with the side of a mother filament and nucleates a new branch (daughter) filament from the pointed end. Formins make long, straight filaments by nucleating and remaining processively associated with elongating filament barbed ends.

In contrast, there is significant uncertainty and disagreement about the mechanisms of the third major class of actin assembly factors, tandem WH2 domain–based nucleators (Dominguez, 2016). Proteins in this group include bacterial (*Rickettsia* Sca2 and *Vibrio* VopL and VopF) and eukaryotic (Cordon-bleu [Cobl] and Spire) actin assembly factors, with different numbers and configurations of actin monomer–binding WH2 domains, proposed to promote filament nucleation and elongation by different mechanisms (Paunola et al., 2002; Dominguez, 2007, 2016; Qualmann and Kessels, 2009; Carlier et al., 2011). Sca2 contains three WH2 domains and promotes actin filament nucleation and elongation by remaining processively associated with the barbed end (Haglund et al., 2010; Madasu et al., 2013). Spire contains four WH2 domains but functions optimally as a dimer, induced by interaction with

formins, and nucleates actin filament assembly from the pointed end (Quinlan et al., 2005, 2007; Rasson et al., 2015). Cobl contains a tandem repeat of three WH2 domains (Ahuja et al., 2007) and was originally identified as an actin nucleator involved in neuronal cell morphogenesis (Ahuja et al., 2007; Haag et al., 2012). However, other studies have produced conflicting models about the activities of Spire and Cobl, concluding that Spire functions mainly as a barbed-end capping protein (CP; Montaville et al., 2014), whereas Cobl is only a weak nucleator and functions primarily as a monomer-sequestering and filament-severing factor (Carlier et al., 2011; Husson et al., 2011).

Another example of disagreement concerns the filament assembly mechanism of VopL and VopF (VopL/F), which are virulence factors from the pathogenic gram-negative bacteria *Vibrio parahaemolyticus* and *Vibrio cholera* (Dominguez, 2016). VopL/F are type III secretion factors that contribute to entry and infection of host intestinal epithelial cells by facilitating nonphysiological actin cytoskeleton rearrangements (Reidl and Klose, 2002; Liverman et al., 2007; Tam et al., 2007, 2010). VopL/F are closely related (32% sequence identity and 72% sequence similarity), and both contain three WH2 domains and a ~240-residue VopL/F C-terminal domain (VCD) that mediates dimerization (Fig. 1 A; Namgoong et al., 2011; Yu et al., 2011). VopL/F induce actin polymerization in cells and nucleate actin assembly in vitro (Liverman et al., 2007; Tam et al., 2007). However, despite their identical domain organization (Fig. 1 A) and similar sequences, studies have reached opposite conclusions

Correspondence to David R. Kovar: drkovar@uchicago.edu

Abbreviations used: CP, capping protein; TIRFM, total internal reflection fluorescence microscopy; VCD, VopL/F C-terminal domain.
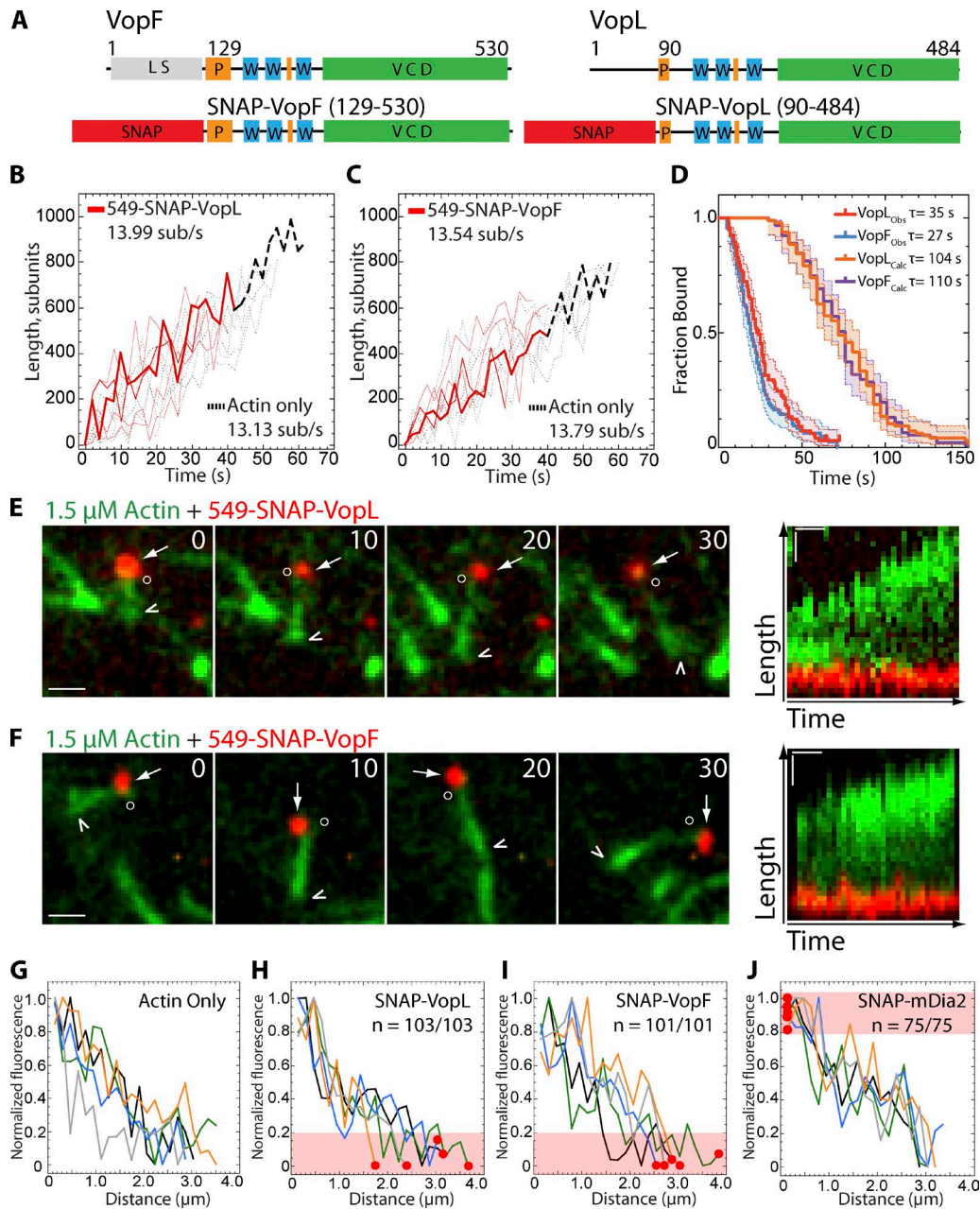
Figure 1. **VopL/F nucleate and then remain briefly associated with the pointed end of an actin filament.** (A) Top, domain organization of VopL/F. Orange, proline-rich region (P); blue, WH2 domain (W); green, VCD dimerization domain. Bottom, VopL/F constructs used in this study with SNAP tag (red) for labeling. (B–J) Slow acquisition (every 2 s, B–D) and rapid acquisition (every second, E–J) two-color TIRFM of the assembly of 1.5 µM Mg-ATP-actin (15% Oregon green actin) with 0.2 nM 549(red)-SNAP-VopL/F. (B and C) Length of individual control (dashed black), 549-SNAP-VopL–associated (B, solid red), or 549-SNAP-VopF-associated (C, solid red) filaments over time ($n \geq 20$). (D) Kaplan–Meier curves representing the mean residence time of 549-SNAP-VopL/F on actin filaments observed ($VopL_{Obs}$, $VopF_{Obs}$) or assumed to have been associated because of nucleation ($VopL_{Calc}$, $VopF_{Calc}$). Error bars indicate 95% CI; $n \geq 90$ events. (E and F, left) Merged time-lapse micrographs (in seconds) of individual filaments. White arrowheads and open circles indicate bright and dim filament ends. White arrows indicate 549-SNAP-VopL/F. (E and F, right) Merged kymographs of filament length (y axis; bar, 1 µm) over time (x axis; bar, 10 s) of the corresponding filaments. Bars, 2 µm. (G–J) Linescans of the normalized fluorescence intensity of individual actin filaments measured from their bright to dim (bleached) ends. Red dots indicate position of 549-SNAP-VopL/F or 549-SNAP-mDia2 on the filament traces, and shaded red regions indicate where 100% of VopL/F or mDia2 are bound to the filaments ($n \geq 75$).

regarding their mechanism of actin assembly (Namgoong et al., 2011; Yu et al., 2011; Pernier et al., 2013; Avvaru et al., 2015).

VopL has been proposed to nucleate actin filament assembly from the pointed end, whereby the WH2 domains and VCD cooperate to bind and nucleate actin monomers, leaving the VCD domain associated briefly with the pointed end of the nascent filament (Namgoong et al., 2011; Yu et al., 2011). A crystal structure of VopL in complex with actin revealed that the VCD dimer organizes three actin subunits into a filament-like conformation, with the VCD bound at the pointed end of this trimeric actin nucleus (Zahm et al., 2013). The WH2 domains are an accessory, contributing to nucleation by delivering actin subunits to the VCD-assembled nucleus (Namgoong et al., 2011; Yu et al., 2011; Zahm et al., 2013). Visualization by total

internal reflection fluorescence microscopy (TIRFM) indicates that VopL associates briefly with the pointed end of the filaments it nucleates (Namgoong et al., 2011). However, ~7.6% of the filaments associated with quantum dot–conjugated VopL buckled and elongated at twice the control rate, indicative of processive barbed end association. These results suggested a "template" nucleation mechanism whereby VopL stimulates rapid (shotgun) cycles of nucleation and associates only briefly with the pointed end of newly formed filaments through its VCD (Namgoong et al., 2011; Yu et al., 2011; Zahm et al., 2013).

In contrast, single-color TIRFM and bulk pyrene-actin assembly studies on VopF led to the conclusion that it sequesters actin monomers and associates exclusively with the barbed end to compete with CP and promote processive elongation (Pernier et al., 2013; Avvaru et al., 2015). Additionally, small-angle x-ray scattering analysis of progressively smaller VopF constructs in complex with actin suggested that VopF stabilizes linear strings of actin subunits, instead of a double-stranded filament (Avvaru et al., 2015). Combined, these results led to a model whereby VopF can associate with the side of a growing filament and potentially ride processively on the barbed end, adding monomers and preventing capping (Pernier et al., 2013).

Here, we sought to resolve this controversy by using multicolor TIRFM to directly observe spontaneous and seeded actin monomer assembly in the presence of fluorescently labeled VopL/F. The results allow us to conclude that VopL/F catalyze actin nucleation by identical pointed-end mechanisms and bind barbed ends only under nonphysiological experimental conditions.

Results and discussion

VopL/F nucleate polymerization and remain briefly associated with the pointed end

We purified VopL/F constructs containing the two proline-rich domains, WH2 domains, and VCD (Fig. 1 A), and lacking only the variable N-terminal region, which is dispensable for actin assembly (Liverman et al., 2007; Namgoong et al., 2011; Pernier et al., 2013). A SNAP-tag was added at the N terminus of each construct for labeling with fluorescent dyes, hereafter referred collectively as SNAP-VopL/F, as the activities of both proteins were nearly indistinguishable in all the assays.

We first compared the activities of untagged, unlabeled, and fluorescently labeled versions of VopL/F by monitoring the assembly of Mg-ATP-actin (10% pyrene actin) in bulk pyrene-actin polymerization assays (Fig. S1). All the proteins accelerated spontaneous actin monomer assembly in a nearly identical way with increasing concentration (Figs. S1, A–C), demonstrating that the SNAP-tag and fluorescent labels do not affect their activities. Moreover, the time to half-maximal pyrene fluorescence agreed well with previous results using unlabeled VopL/F constructs (Liverman et al., 2007; Tam et al., 2007; Namgoong et al., 2011; Pernier et al., 2013).

We then used multicolor TIRFM to directly visualize actin assembly by fluorescently labeled SNAP-VopL/F. We monitored the assembly of 1.5 µM Mg-ATP-actin monomers (15% Oregon-green actin) with 0.2 nM red-labeled 549-SNAP-VopL/F (Fig. S1, E and F; and Video 1). 549-SNAP-VopL/F nucleate actin polymerization and remain bound to one end of the actin filament as it begins to elongate. Proteins that remain continuously associated with elongating barbed ends, such as formin (Kovar, 2006), typically modify the elongation rate. By comparison, fil-

aments associated with 549-SNAP-VopL/F elongated at a rate of ~13.0 subunits per second (sub s^{-1}), indistinguishable from the elongation rates of control filaments and filaments dissociating from 549-SNAP-VopL/F (Fig. 1, B and C). We also confirmed that VopL/F function as dimers, as reported (Namgoong et al., 2011; Pernier et al., 2013; Zahm et al., 2013), because 88% of the 549-SNAP-VopL/F molecules on nucleated filaments photobleached in two or fewer steps, as predicted based on a labeling efficiency of ~75% (Figs. S1, G and H).

The mean time that 549-SNAP-VopL/F remained associated with nucleated filaments before dissociation was 27–34 s (Fig. 1 D, red and blue traces). However, these filaments are not visible immediately after nucleation because of the dead time required for the reaction to flow into the chamber (~20 s) and for filaments to reach an observable length (~0.5 µm). Therefore, assuming that VopL/F were bound to these filaments from their inception (nucleation), we determined their actual mean residence time to be ~110 s (Fig. 1 D, orange and purple traces), during which time ~1,400 actin subunits were added to the filaments. Higher oligomeric states of 549-SNAP-VopL/F do not correlate with increased residence times (Fig. S1 I). We conclude that in spontaneous actin monomer assembly reactions, individual VopL/F dimers display exclusively actin nucleation activity (not elongation or capping) and remain associated with one end of the filament for a short time of ~110 s.

The pointed ends of actin filaments assembled from fluorescently labeled monomers bleach much faster than their barbed ends, to which fresh subunits add at a faster rate (Fig. S2 A; Kovar and Pollard, 2004). Thus, we imaged TIRFM reactions rapidly (1 frame/s) to observe spontaneous actin assembly with 549-SNAP-VopL/F (Fig. 1, E and F; and Video 2). Linescans of filament fluorescence revealed a steady decrease in intensity from the barbed to the pointed end (Fig. 1, G–J). VopL/F were always bound to the dimmer, pointed end of nucleated filaments (Fig. 1, H and I, $n \geq 101$). Conversely, the formin mDia2 (549-SNAP-mDia2), a well-known barbed-end actin assembly factor, localized exclusively to the bright, barbed end of actin filaments (Figs. 1 J and S2 B; and Video 2; Kovar, 2006).

We can rule out the possibility that the SNAP-tag artificially induces VopL/F-mediated pointed-end nucleation, because fluorescently labeled CP (647-SNAP-CP) bound similarly to the barbed ends of filaments nucleated by untagged VopL and 549-SNAP-VopL (Fig. S1 D). Furthermore, C-terminally tagged VopL/F-SNAP-549 (Fig. S2, C–E) and 549-SNAP-VopL, at a range of concentrations (200–800 pM; Fig. S2 F), also nucleated exclusively from the pointed end, demonstrating that the position of the tag and protein concentration do not alter the nucleation behavior of VopL/F.

Formin and CP bind simultaneously with VopL/F to the opposite end of the filament

Given that VopL/F are pointed-end nucleators, the barbed-end binding proteins formin and CP should bind to the opposite end. We used three-color TIRFM to directly visualize the assembly of 1.5 µM Mg-ATP-actin (15% Oregon green actin) monomers with 549-SNAP-VopL/F and cyan-labeled CP (647-SNAP-CP) or mDia2 (647-SNAP-mDia2; Fig. 2). As expected, in 100% of our observations, 647-SNAP-mDia2 and 647-SNAP-CP associated with the opposite end of 549-SNAP-VopL/F-nucleated actin filaments (Fig. 2, A–E). Furthermore, 647-SNAP-mDia2 and 647-SNAP-CP never appeared to dissociate or replace 549-SNAP-VopL/F at the pointed end (not depicted).
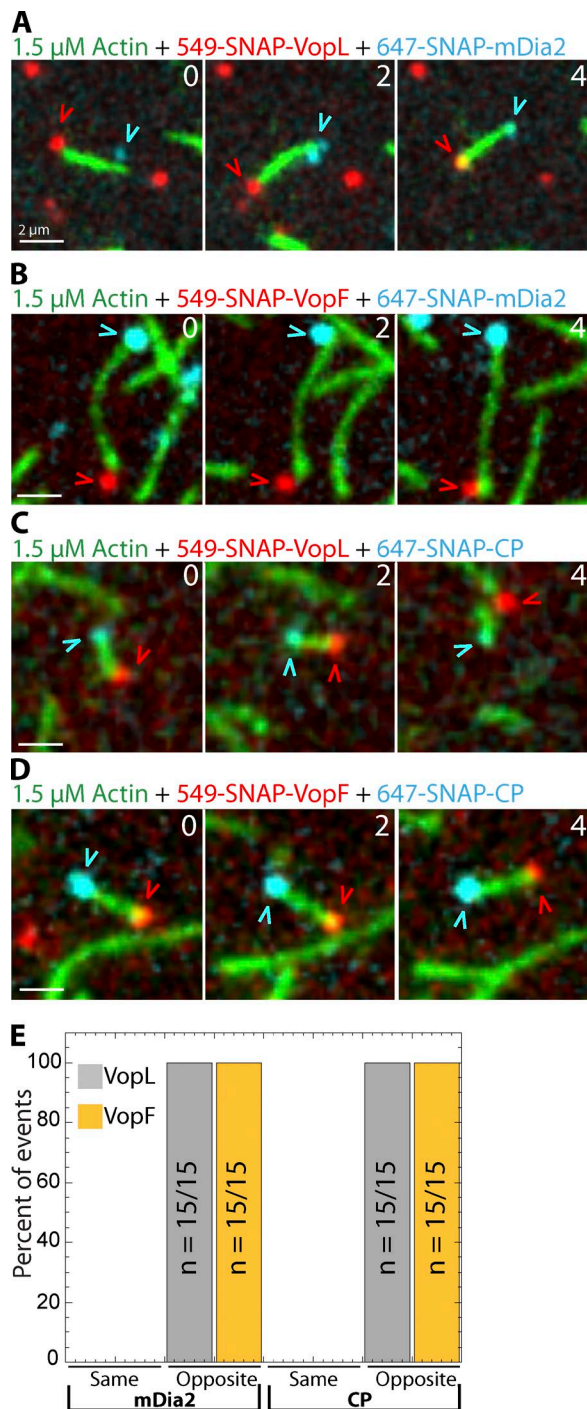
Figure 2. **Formin mDia2 and CP bind the opposite end of VopL/F-nucleated filaments.** Three-color TIRFM of the assembly of 1.5 µM Mg-ATP-actin (15% Oregon green actin) assembled with 0.2 nM 549 (red)-SNAP-VopL/F and either 2 nM 647 (cyan)-SNAP-mDia2 or 2 nM 647-SNAP-MmCP. (A–D) Merged time-lapse micrographs (in seconds) of individual filaments. Bars, 2 µm. Red and blue arrowheads indicate 549-SNAP-VopL/F and 647-SNAP-mDia2/647-SNAP-MmCP. (E) Percentage of filaments in which 549-SNAP-VopL (gray) or 549-SNAP-VopF (gold) are on the same or opposite end as mDia2 or MmCP. *n* = 15.

Without actin monomers, VopL/F can bind both ends of preassembled actin filaments

In the presence of actin monomers, VopL/F bind exclusively to the pointed end of the filaments they nucleate (Figs. 1 and

2) and, unlike mDia2, were never observed to either bind the ends of spontaneously assembled control filaments or rebind to the ends of the filaments from which they had dissociated after nucleation. These observations contradict a previous study that VopF binds to both free and capped barbed ends (Pernier et al., 2013). To explore this question further, we directly tested the ability of VopL/F to bind preassembled filament ends (Fig. 3 and Video 3). Actin filaments were preassembled in a TIRFM chamber from 1.5 µM Mg-ATP-actin (10% Alexa Fluor 488 actin), and 549-SNAP-VopL/F (Fig. 3, A and C) or 549-SNAP-mDia2 (Fig. 3, B and D) was flowed in with or without 1.5 µM Mg-ATP-actin monomers (10% Alexa Fluor 488 actin). The presence of actin monomers resulted in a marked difference in the lengths of filaments bound by 549-SNAP-VopL/F compared with 549-SNAP-mDia2 (Fig. 3, A, B, and E; and Video 3). mDia2 associates with the barbed ends of the filaments it nucleates and to preassembled filaments (Kovar et al., 2006). 549-SNAP-mDia2 was observed bound to filaments with a large distribution of lengths, including shorter, nucleated filaments and longer, preassembled filaments (Fig. 3, B and E, mDia2 red dots). Consistent with our previous observations (Figs. 1 and 2), 549-SNAP-VopL/F exclusively associated with one end of shorter (~1.5-µm-long) nucleated filaments (Fig. 3, A and E, VopL/F red dots).

In contrast, both 549-SNAP-VopL/F and 549-SNAP-mDia2 bound preassembled filaments ends when actin monomers were not included in the reaction (Fig. 3, C and D; and Video 4). 549-SNAP-mDia2 bound the barbed end of preassembled filaments with a broad length distribution (Fig. 3 E, mDia2 black dots), and in 117 of 118 observations, it remained bound throughout the 10-min experiment. Similarly, 549-SNAP-VopL/F (Fig. 3 C) can bind preassembled actin filament ends in the absence of actin monomers (Fig. 3 E, VopL/F black dots). However, VopL/F associate with both barbed and pointed ends, with no significant preference (Fig. 3, F and H), and with a mean residence time of ~25–30 s (Fig. 3, G and H).

In the presence of profilin, VopL/F primarily nucleate and remain briefly associated with the pointed end

Because cells contain a mixture of actin filaments and monomers that are mostly bound to profilin, we modified the preassembled actin filament TIRFM assay. Green actin filaments were preassembled in a TIRFM chamber from 1.5 µM Mg-ATP-actin monomers (10% Alexa Fluor 488 actin). Red-labeled assembly factors (549-SNAP-VopL/F or 549-SNAP-mDia2) were then flowed into the chamber with 1.5 µM cyan Mg-ATP-actin monomers (10% Alexa Fluor 647 actin) in either the absence or presence of profilin at a 2:1 (3.0 µM) or 5:1 (7.5 µM) molar ratio to actin monomers (as described in Fig. 4 A). This setup reveals whether the assembly factors associate with cyan-colored newly nucleated filaments or green/cyan-colored preassembled filaments, whose barbed ends elongate from cyan-labeled actin (Fig. 4 A, right).

From such reactions (Fig. 4 B), we were able to quantify the following: (a) the percentage of nucleated or preassembled filaments associated with assembly factors (Fig. 4 C); (b) the lifetimes of association of assembly factors with nucleated and preassembled filament ends (Fig. 4 D), and (c) the barbed-end elongation rates of nucleated and preassembled filaments associated with assembly factors (Fig. 4 E). In the absence of profilin, VopL/F associated exclusively with the bleached pointed ends of the filaments they nucleated (Fig. 4 C) for ~80 s (Fig. 4 D),
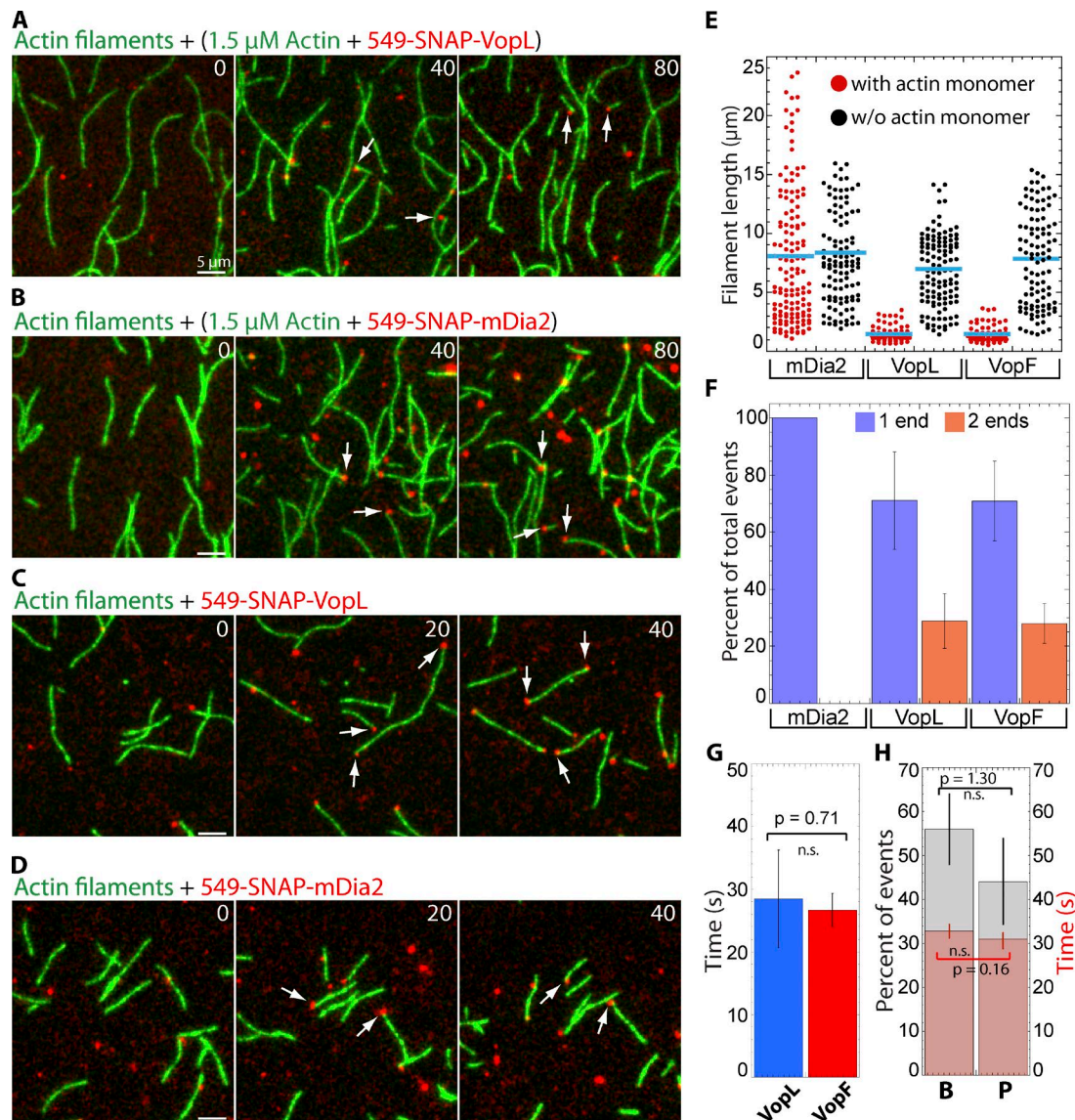
Figure 3. In the absence of actin monomers, VopL/F bind preassembled filament ends. Two-color TIRFM visualization of the addition of 0.6 nM 549-SNAP-VopL/F to preassembled actin filaments (10% Alexa Fluor 488 actin) in the absence and presence of 1.5 µM Mg-ATP-actin (10% Alexa Fluor 488 actin) monomers. (A–D) Merged time-lapse micrographs (in seconds) of filaments upon flow-in (time zero) of 549-SNAP-VopL or formin 549-SNAP-mDia2 with and without actin monomers, as indicated. White arrows mark VopL and mDia2. Bars, 5 µm. (E) Length distribution of bound filaments in the presence (red) and absence (black) of actin monomers. Blue lines indicate mean filament length. $n \geq 50$ events. (F) Percentage of filaments that are bound on one (purple) or two (orange) ends. Error bars indicate SD; $n \geq 50$. (G) Mean association time of 549-SNAP-VopL/F on actin filament ends in the absence of monomer. Error bars indicate SEM; $n \geq 100$ events. (H) Percentage of 549-SNAP-VopL binding events that are on the barbed (B) or pointed (P) end (gray columns), and mean association time of 549-SNAP-VopL on either the barbed or pointed end (red columns). Error bars indicate SEM; $n \geq 100$ events.

which elongated at the control barbed end rate of ~10 sub s^{-1} (Fig. 4 E). In contrast, mDia2 associated with the barbed ends of both nucleated and preassembled filaments (Fig. 4 C), slowing the barbed end elongation rate to ~2.5 sub s^{-1} (Fig. 4 E; Kovar et al., 2006). In the presence of two- or fivefold molar excess of profilin to actin monomers (Fig. 4 B), the vast majority (85–95%) of VopL/F also associated with the pointed end of newly nucleated filaments (Fig. 4 C) for ~80 s (Fig. 4 D), which elongated at ~10 sub s^{-1} (Fig. 4 E). However, in these reactions, 5–15% of the VopL/F association events were with the barbed ends of preassembled actin filaments (Fig. 4 C and Video 5) for ~25 s (Fig. 4 D), in which case barbed-end elongation is essentially capped (Fig. 4 E). In contrast to flow-in experiments without actin monomers (Fig. 3), VopL/F were not observed to

interact with the pointed end of preassembled actin filaments in the presence of profilin. Inclusion of profilin also slightly increased the percentage of mDia2 associated with preassembled filaments (Fig. 4 C), likely because of profilin's inhibition of formin-mediated nucleation (Kovar et al., 2003). In conclusion, even if the presence of a large excess of profilin allows VopL/F to associate with and cap filament barbed ends (Pernier et al., 2013), the vast majority of observations (~85%) correspond to nucleation events from the pointed end.

VopL and VopF share actin assembly and association properties

Previous studies reported opposite actin assembly mechanisms for the closely related *Vibrio* virulence factors VopL and VopF;
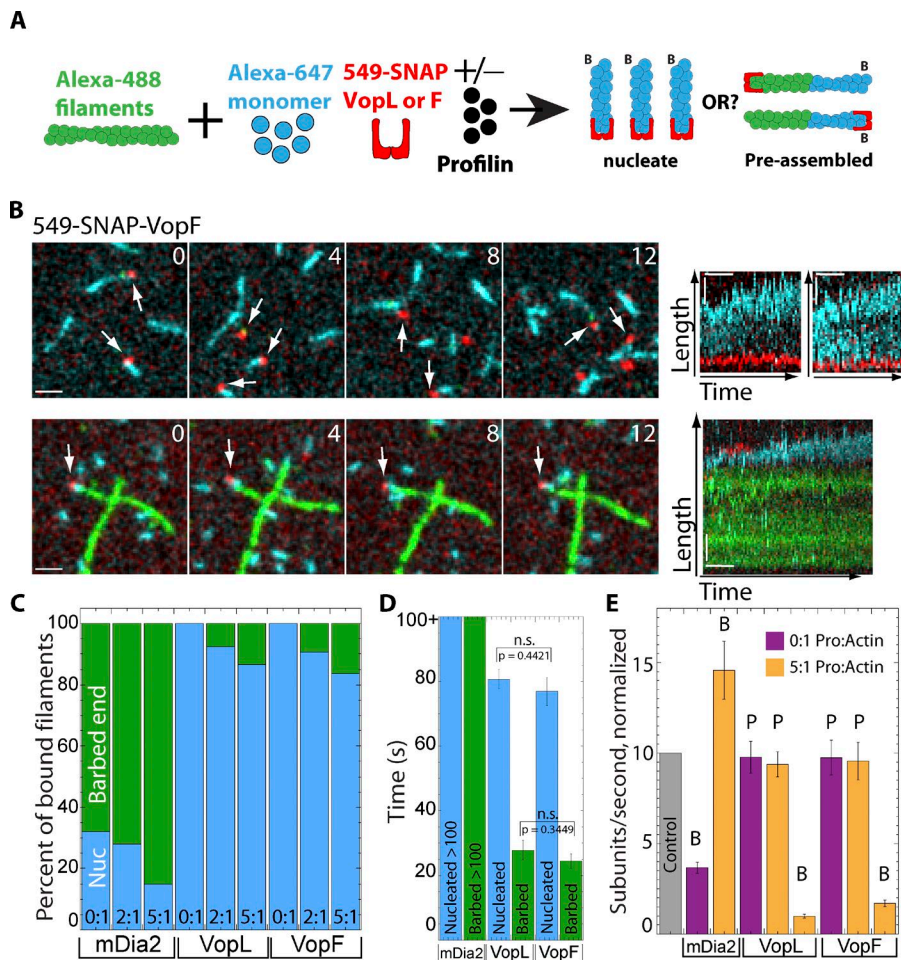
Figure 4. **VopL/F on the ends of nucleated and preassembled filaments in the presence of profilin.** Three-color TIRFM visualization of the addition of 1.5 µM cyan-labeled Mg-ATP-actin monomers (15% Alexa Fluor 647 actin) to preassembled green actin filaments (10% Alexa Fluor 488 actin), in the presence of 0.2 nM 549(red)-SNAP-VopF/L or 549-SNAP-mDia2, with 0, 3.0, or 7.0 µM profilin HsPRFN1. (A) Cartoon of the experiment and potential outcomes. (B) Flow (time zero) of 549-SNAP-VopF in the presence of 7.0 µM profilin. Left, merged time-lapse micrographs (in seconds) of actin filaments. White arrows indicate 549-SNAP-VopF. Bar, 2 µm. Right, kymographs of filament length (y axis; bar, 2 µm) over time (x axis; bar, 10 s) of the corresponding filaments. Top, examples of the predominant filament population, association of 549-SNAP-VopF with the pointed end of nucleated filaments. Bottom, example of 549-SNAP-VopF binding to the barbed end of a preassembled filament. (C) Percentage of 549-SNAP-mDia2 or 549-SNAP-VopL/F associated with nucleated filaments (blue; pointed end for VopL/F, barbed end for mDia2) or preassembled filament barbed ends (green) for different profilin:actin ratios (0:1, 2:1, 5:1; $n \geq 50$). (D) Mean association time of 549-SNAP-VopL/F or 549-SNAP-mDia2 with the barbed end of preassembled filaments with a 5:1 profilin:actin ratio. Error bars indicate ± SEM; $n \geq 20$ events. (E) Normalized elongation rates of 549-SNAP-mDia2- or 549-SNAP-VopL/F-associated filaments with a 0:1 (purple) or 5:1 (yellow) ratio of profilin/actin. B/P, barbed/pointed end. Error bars indicate ± SEM; $n = 20$ filaments.

VopL exclusively nucleated polymerization from the pointed end (Namgoong et al., 2011; Zahm et al., 2013), whereas VopF exclusively bound to the barbed end of preassembled actin filaments (Pernier et al., 2013; Avvaru et al., 2015). By addressing this discrepancy, we discovered here that VopL/F share a multifunctional mechanism of actin filament assembly and association (Fig. 5). The vast majority of filament assembly events, with or without saturating profilin, converge on a pointed-end nucleation mechanism for VopL and VopF (Namgoong et al., 2011; Yu et al., 2011; Zahm et al., 2013; Fig. 5, A and C). Furthermore, our experiments can reproduce all the filament association modes previously reported for VopL/F (Namgoong et al., 2011; Pernier et al., 2013; Zahm et al., 2013; Avvaru et al., 2015) and reveal that the reaction conditions critically determine whether VopL/F associate with different filament ends.

We propose that the primary mechanism of actin filament assembly by VopL/F is as follows. The WH2 domains recruit actin monomers to the VCD, which organizes three monomers into a nucleus (Zahm et al., 2013). VopL/F remain briefly bound to the pointed end via the VCD domain, whereas the WH2 domains dissociate to allow the nucleus to elongate from the barbed end (Fig. 5 A). After detachment of the WH2 domains, the affinity of VCD alone for the pointed end is relatively weak, which at least in part explains the dissociation of VopL/F after only ∼100 s. Upon dissociation, VCD might carry actin subunits with it, which can act as a new nucleation center, overcoming inhibition of nucleation by

profilin; or alternatively, the VCD could reload profilin-free monomers from solution.

Unlike other F-actin end-binding proteins, such as formins and CP, VopL/F can bind the ends of preassembled filaments only under nonphysiological conditions, including in the total absence of actin monomers, where they can bind to both the barbed and pointed end (Fig. 5 B), or infrequently (<15% of events), when actin monomers are fully saturated with profilin, where they can bind only to the barbed end (Fig. 5 C). The VCD domain likely facilitates association of VopL/F with preassembled pointed ends (Fig. 5 B; Namgoong et al., 2011; Zahm et al., 2013), whereas the WH2 domains might mediate binding to the barbed end of preassembled filaments (Fig. 5, A and C). Indeed, although the WH2 domain preferentially binds actin monomers, if monomers are omitted from the reaction or the binding site of the WH2 domain on the actin monomer is masked by excess profilin, they might bind to the barbed end of the filament, which is the only location along the filament where the binding site of the WH2 domain is fully exposed (Chereau et al., 2005; Dominguez, 2010, 2016). Finally, why do VopL/F not bind to the pointed end of preassembled filaments in the presence of saturating profilin? Under these conditions, profilin and profilin-actin likely saturate the proline-rich domains of VopL/F, which may sterically hinder binding to the pointed end. Together, the preferential binding of VopL/F to actin monomers, their quick detachment from the pointed end of newly assembled filaments, and their negligible binding to preformed filaments

A
VopL/VopF + G-actin

B
VopL/VopF + F-actin

C
VopL/VopF + Profilin-actin and F-actin
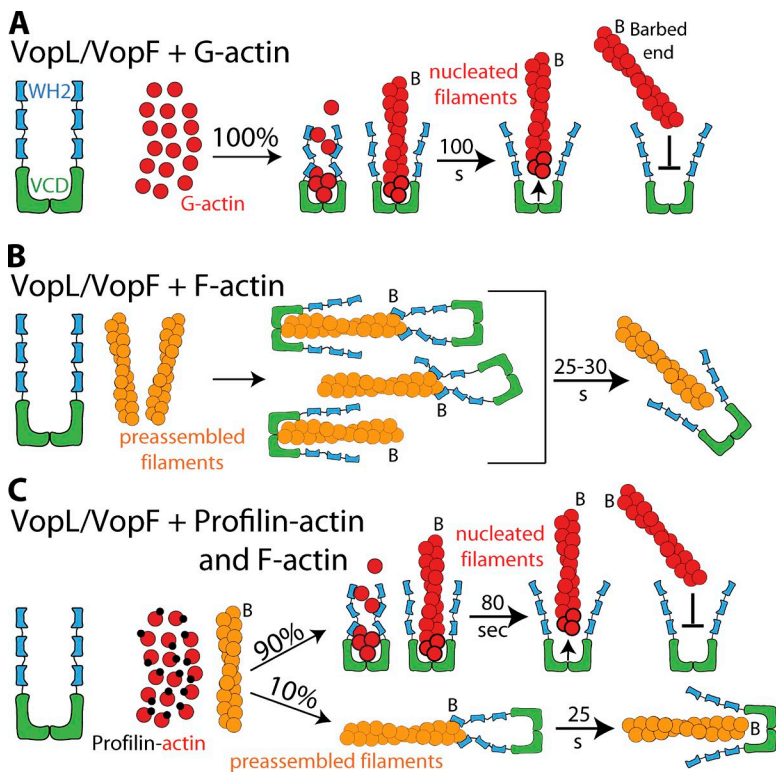
Figure 5. **Summary of VopL/F-mediated actin filament nucleation and association over a range of experimental conditions.** Cartoon representation of VopL/F's actin assembly properties with actin monomers (A), preassembled filaments only (B), and preassembled filaments with actin monomers and profilin (C). VopL/F are illustrated as a generalized dimer (A–C, left). (A) The VopL/F WH2 domains recruit actin monomers to the VCD, which organizes three monomers into an F-actin nucleus (red circles with bold outlines). The VCD domain remains briefly (~100 s) associated with the pointed end, and VopL/F are unable to rebind or associate with preassembled filament ends. (B) In the absence of actin monomers, VopL/F can bind preassembled actin filament ends for ~25–30 s. The VCD and WH2 domains mediate interaction with pointed and barbed ends, respectively. (C) In the presence of profilin-actin, VopL/F primarily (~90%) nucleates actin filaments and then remains briefly (~80 s) associated with the pointed end. VopL/F occasionally (10%) associates with preassembled filament barbed ends through their WH2 domains.

converge to favor nucleation as their main activity under physiological conditions.

Our results explain some of the disagreement among previous studies, as some of the experiments were performed with a 5:1 profilin:actin ratio. However, it is unclear how the studies on VopF failed to observe pointed-end binding (Pernier et al., 2013; Avvaru et al., 2015). We found that pointed-end nucleation is the only mechanism for VopL/F in the presence of actin monomers, whereas in the absence of actin monomers, VopL/F bind to both filament ends, and even with saturating profilin, the vast majority of events (~85%) correspond to pointed-end nucleation.

The cartoon representing our combined results of actin filament nucleation and association by VopL/F (Fig. 5) agrees well with in vivo studies (Liverman et al., 2007; Tam et al., 2007, 2010). The primary function of VopL/F is to promote virulence of the *Vibrio* bacteria through efficient pointed-end nucleation of unproductive actin filaments in the host cell (Fig. 5, A and C). Given that the concentration of actin monomers in *Vibrio*'s preferred hosts (higher eukaryotes) can be as high as 100 µM (Pollard et al., 2000), VopL/F will primarily drive efficient pointed-end nucleation. Furthermore, even if actin monomers are outnumbered 5:1 by profilin (Goldschmidt-Clermont et al., 1991, 1992; Wühr et al., 2014), pointed-end nucleation should predominate (Figs. 4 and 5 C). Assembly of unproductive F-actin decreases the concentration of actin monomers in host cells to the detriment of endogenous F-actin networks. Both in vitro electrophysiological and in vivo mouse colonization results indicate that VopF negatively affects F-actin–dependent tight-junction integrity in intestinal epithelial cells (Balda and Matter, 2008; Tam et al., 2010), which can lead to intestinal inflammation, rapid fluid loss, and passing of the *Vibrio* bacteria (Faruque et al., 1998; Reidl and Klose, 2002).

Materials and methods

Plasmid construction

VopL/F constructs were prepared by infusion (Takara Bio Inc.) after PCR amplification (iProof; Bio-Rad Laboratories) from plasmid DNA for VopL and from codon-optimized plasmid DNA for VopF (provided by E. Kerkhoff, University of Regensburg, Regensburg, Germany), with a 6xHis tag included in the reverse primer. PCR products were cloned into the SNAP-tag-T7-2vector (New England Biolabs, Inc.) at the XmaI/PacI sites, but the PacI site is not maintained. A flexible linker (GGSGGS) was included in the forward primer sequences of the SNAP constructs between the SNAP and the VopL/F DNA sequences.

Protein expression and purification

Recombinant SNAP-VopL/F-6xHIS, VopL/F-SNAP-6xHIS, SNAP-MmDia2 (521-1171, FH1-C)-6xHIS (SNAP-mDia2), and mouse CP (dual-expression construct of MmCP α1-6xHIS and SNAP-β2; SNAP-CP) proteins were purified from *Escherichia coli* strain BL21-Codon Plus (DE3)-RP (Agilent Technologies), after their expression with 0.5 mM isopropyl β-D-1-thio-galactopyranoside for 16 h at 16°C. Cells were lysed with an Emulsi-Flex-C3 (Avestin) in extraction buffer (50 mM NaH_2PO_4, pH 8.0, 500 mM NaCl, 10% glycerol, 10 mM imidazole, and 10 mM β-mercaptoethanol) and were clarified by centrifugation at 16,000 rpm for 15 min, followed by 18,000 rpm for 30 min, in a Beckman SS-34 rotor. The extract was incubated for 1 h at 4°C with Talon Resin (Takara Bio Inc.), loaded onto a column, and washed with extraction buffer, and all proteins were eluted with 250 mM imidazole. SNAP-VopL/F and SNAP-mDia2 were dialyzed against buffer (20 mM Hepes, pH 7.4, 200 mM KCl, 0.01% NaN_3, and 1 mM DTT). SNAP-CP was dialyzed against CP buffer (10 mM Tris, pH 7.5, 40 mM KCl, 50% glycerol, 0.5 mM DTT, and 0.01% NaN_3). SNAP-tagged VopL/F were labeled with SNAP-Surface 549, and SNAP-mDia2 and SNAP-CP

were labeled with SNAP Surface 549 or 647 according to the manufacturers' protocols (New England Biolabs, Inc.). Concentrations of SNAP-tagged proteins and the degree of labeling were determined by densitometry of Coomassie-stained bands on SDS-PAGE gels compared with standards and by measuring fluorophore absorbance in solution using the extinction coefficient of SNAP-surface549: $\varepsilon_{560} = 150,000$ M/cm. VopL/F were flash-frozen in liquid nitrogen and stored at −80°C. Actin was purified from chicken skeletal muscle acetone powder by a cycle of polymerization and depolymerization and gel filtration (Spudich and Watt, 1971). Gel-filtered actin was labeled on Cys374 with Oregon green iodoacetamide (Thermo Fisher Scientific; Kuhn and Pollard, 2005) or on surface lysines with Alexa Fluor 488 or Alexa Fluor 647 succinimidylester (Thermo Fisher Scientific; McCullough et al., 2011; Kang et al., 2012). Additional information about protein purification for mouse CP can be found in Palmgren et al. (2001), and for formin mDia2, in Suarez et al. (2015).

Glass preparation
Microscope slides and coverslips (#1.5; Thermo Fisher Scientific) were washed successively for 10 min each with (1) acetone, (2) isopropanol, (3) MilliQ H_2O, and (4) isopropanol. They were then sonicated for 30 min with isopropanol, incubated for 1 h with piranha solution (80% H_2SO_4 and 20% H_2O_2), washed with deionized water, then washed with isopropanol and dried. Glass was incubated for 18 h with 1 mg/ml mPeg-Silane (5,000 MW) in 95% ethanol, pH 2.0. Slides were washed once with 95% ethanol and then five times with MilliQ H_2O, air dried, and stored in Petri dishes at 4°C. Parallel strips of double-sided tape were placed on the coverslip to create multiple flow chambers (Zimmermann et al., 2016).

TIRFM image acquisition
TIRFM images were collected at 1- to 4-s intervals with an iXon EMC CD camera (Andor Technology) using an Olympus IX-71 microscope fitted with through-the-objective TIRFM illumination with an Olympus 60× 1.49-NA oil objective controlled by MetaMorph Basic Version 7.8.2.0 (Molecular Devices) at 22°C (Zimmermann et al., 2016). Mg-ATP-actin (15% Oregon green actin) was mixed with 2× TIRF buffer (1× = 10 mM imidazole, pH 7.0, 50 mM KCl, 1 mM $MgCl_2$, 1 mM EGTA, 50 mM DTT, 0.2 mM ATP, 50 µM $CaCl_2$, 15 mM glucose, 20 µg/ml catalase, 100 µg/ml glucose oxidase, and 0.5% [400 centipoise] methylcellulose) and SNAP-VopL/F and transferred to a flow cell for imaging at 23°C. For two- and three-color TIRFM, we cyclically imaged Oregon green actin or Alexa Fluor 488 actin (one frame, 488-nm excitation for 50 ms), 549-SNAP-VopL/F (one frame, 561-nm excitation for 50 ms), and 647-SNAP-CP, 647-SNAP-mDia2, or Alexa Fluor 647 actin (one frame, 640-nm excitation for 50 ms).

Photobleaching and analysis of fluorescence intensity
For photobleaching experiments to determine the oligomerization state of VopL/F, 549-SNAP-VopL/F were imaged continuously, whereas actin filaments were imaged intermittently (Winkelman et al., 2014). Specifically, TIRFM images were collected continuously (10–20 frames/s) in the 561-nm channel, with the 488-nm shutter opened every 20–40 frames to visualize actin. The observed distribution of photobleaching steps was compared with the number of steps predicted by a binomial distribution model where $s = 0.75$ (Breitsprecher et al., 2012). When spots did not bleach completely, the number of fluorescent subunits present was inferred by intensity and step size. Background fluorescence was subtracted with ImageJ using a rolling ball radius of 30 pixels, and the integrated fluorescence signals of 549-SNAP-VopL/F spots associated with the end of actin filaments were manually tracked and measured using ImageJ.

Calculation of residence time and measuring the lengths of bound filaments
To calculate residence times on actin filament ends in all conditions, 549-SNAP-VopL/F spots associated with filament ends were tracked manually in ImageJ (Winkelman et al., 2014). Residence times for 549-SNAP-VopL/F on nucleated actin filaments in spontaneous TIR FM assays in Figs. 1 D and 4 D were determined through back-calculation by measuring the length of actin filaments immediately before the 549-SNAP-VopL/F dissociated and converting that length into total actin subunits (1 µm = 375 subunits). The subunit length was divided by the mean elongation rate of the filaments. Barbed-end elongation rates were calculated by measuring filament lengths over time with ImageJ. Lengths of actin filaments for the dot plot in Fig. 3 E were measured in ImageJ immediately upon binding by 549-SNAP-VopL/F or 549-SNAP-mDia2. We deemed an event to be bound if 549-SNAP-VopL/F or 549-SNAP-mDia2 colocalized with the end of a filament for at least two frames.

Quantification of partially bleached filaments
Partially bleached actin filaments were quantified by using the linescan function in ImageJ. A line was drawn down the length of the filament at the last frame in which a 549-SNAP-VopL/F or 549-SNAP-mDia2 was associated in the RGB merged image and saved as an region of interest (ROI). These ROIs were imported into the 488-channel time lapse (with background subtracted), and a linescan was taken at this point. The raw values were normalized from 0 to 1 for each individual filament. To account for noise, the mean was taken of the three normalized values proximal or distal to the 549-SNAP-VopL/F or 549-SNAP-mDia2. If the mean of the normalized values was less than 0.2 it was considered to be in the dimmest 20% of the filament, and if the value was higher than 0.8 it was considered to be in the brightest 20%. All 549-SNAP-VopL/F events were bound to the dimmest 20%, whereas all 549-SNAP-mDia2 events were bound to the brightest 20%.

Fluorescence spectroscopy
Bulk actin assembly was measured from the fluorescence of pyrene-actin with a Safire2 (Tecan) fluorescent plate reader (Neidt et al., 2008). In brief, the assembly of 10% pyrene-labeled Mg-ATP-actin monomers was initiated by the addition of 50 mM KCl, 1 mM $MgCl_2$, 1 mM EGTA, 10 mM imidazole, pH 7.0, and other proteins to be assayed. Final protein concentrations are indicated in the figure legends.

Online supplemental material
Fig. S1 shows that the SNAP-tag does not affect VopL/F's activities via bulk pyrene-actin assembly assays and three-color TIRFM as well as the photobleaching of 549-SNAP-VopL/F molecules from in vitro TIRFM. Fig. S2 shows that VopL/F-SNAP-549 (C-terminally tagged constructs) localize to the dim, pointed end of partially bleached fluorescently labeled actin filaments. In Videos 1–5, all actin filaments are fluorescently labeled and visualized with multicolor TIRFM. Video 1 (related to Fig. 1) shows 549-SNAP-VopL/F localize to one end of actin filaments. Video 2 (related to Fig. 1 and Fig. S2) shows that 549-SNAP-VopL/F are on the dim, pointed end of partially bleached actin filaments versus the formin 549-SNAP-mDia2, which localizes to the bright, barbed end. Video 3 (related to Fig. 3) shows that 549-SNAP-VopL nucleates only short actin filaments, compared with the formin 549-SNAP-mDia2, which can both nucleate and bind long preassembled actin filaments in the presence of actin monomers. Video 4 (related to Fig. 3) shows that 549-SNAP-VopL binds to both ends of preassembled actin filaments in the absence of actin monomers. Video 5 (related to Fig. 4) shows that 549-SNAP-VopF primarily nucleates actin filaments in the presence of saturating profilin, but also occasionally binds to the barbed end of preassembled actin filaments.

References

Ahuja, R., R. Pinyol, N. Reichenbach, L. Custer, J. Klingensmith, M.M. Kessels, and B. Qualmann. 2007. Cordon-bleu is an actin nucleation factor and controls neuronal morphology. *Cell.* 131:337–350. http://dx.doi.org/10.1016/j.cell.2007.08.030

Avvaru, B.S., J. Pernier, and M.F. Carlier. 2015. Dimeric WH2 repeats of VopF sequester actin monomers into non-nucleating linear string conformations: An X-ray scattering study. *J. Struct. Biol.* 190:192–199. http://dx.doi.org/10.1016/j.jsb.2015.03.008

Balda, M.S., and K. Matter. 2008. Tight junctions at a glance. *J. Cell Sci.* 121:3677–3682. http://dx.doi.org/10.1242/jcs.023887

Blanchoin, L., R. Boujemaa-Paterski, C. Sykes, and J. Plastino. 2014. Actin dynamics, architecture, and mechanics in cell motility. *Physiol. Rev.* 94:235–263. http://dx.doi.org/10.1152/physrev.00018.2013

Breitsprecher, D., R. Jaiswal, J.P. Bombardier, C.J. Gould, J. Gelles, and B.L. Goode. 2012. Rocket launcher mechanism of collaborative actin assembly defined by single-molecule imaging. *Science.* 336:1164–1168. http://dx.doi.org/10.1126/science.1218062

Campellone, K.G., and M.D. Welch. 2010. A nucleator arms race: Cellular control of actin assembly. *Nat. Rev. Mol. Cell Biol.* 11:237–251. http://dx.doi.org/10.1038/nrm2867

Carlier, M.F., C. Husson, L. Renault, and D. Didry. 2011. Control of actin assembly by the WH2 domains and their multifunctional tandem repeats in Spire and Cordon-Bleu. *Int. Rev. Cell Mol. Biol.* 290:55–85. http://dx.doi.org/10.1016/B978-0-12-386037-8.00005-3

Chereau, D., F. Kerff, P. Graceffa, Z. Grabarek, K. Langsetmo, and R. Dominguez. 2005. Actin-bound structures of Wiskott-Aldrich syndrome protein (WASP)-homology domain 2 and the implications for filament assembly. *Proc. Natl. Acad. Sci. USA.* 102:16644–16649. http://dx.doi.org/10.1073/pnas.0507021102

Chesarone, M.A., and B.L. Goode. 2009. Actin nucleation and elongation factors: Mechanisms and interplay. *Curr. Opin. Cell Biol.* 21:28–37. http://dx.doi.org/10.1016/j.ceb.2008.12.001

Chhabra, E.S., and H.N. Higgs. 2007. The many faces of actin: Matching assembly factors with cellular structures. *Nat. Cell Biol.* 9:1110–1121. http://dx.doi.org/10.1038/ncb1007-1110

Dominguez, R. 2007. The beta-thymosin/WH2 fold: Multifunctionality and structure. *Ann. N. Y. Acad. Sci.* 1112:86–94. http://dx.doi.org/10.1196/annals.1415.011

Dominguez, R. 2010. Structural insights into de novo actin polymerization. *Curr. Opin. Struct. Biol.* 20:217–225. http://dx.doi.org/10.1016/j.sbi.2009.12.012

Dominguez, R. 2016. The WH2 domain and actin nucleation: Necessary but insufficient. *Trends Biochem. Sci.* 41:478–490. http://dx.doi.org/10.1016/j.tibs.2016.03.004

Faruque, S.M., M.J. Albert, and J.J. Mekalanos. 1998. Epidemiology, genetics, and ecology of toxigenic *Vibrio cholerae. Microbiol. Mol. Biol. Rev.* 62:1301–1314.

Goldschmidt-Clermont, P.J., J.W. Kim, L.M. Machesky, S.G. Rhee, and T.D. Pollard. 1991. Regulation of phospholipase C-gamma 1 by profilin and tyrosine phosphorylation. *Science.* 251:1231–1233. http://dx.doi.org/10.1126/science.1848725

Goldschmidt-Clermont, P.J., M.I. Furman, D. Wachsstock, D. Safer, V.T. Nachmias, and T.D. Pollard. 1992. The control of actin nucleotide exchange by thymosin beta 4 and profilin. A potential regulatory mechanism for actin polymerization in cells. *Mol. Biol. Cell.* 3:1015–1024. http://dx.doi.org/10.1091/mbc.3.9.1015

Haag, N., L. Schwintzer, R. Ahuja, N. Koch, J. Grimm, H. Heuer, B. Qualmann, and M.M. Kessels. 2012. The actin nucleator Cobl is crucial for Purkinje cell development and works in close conjunction with the F-actin binding protein Abp1. *J. Neurosci.* 32:17842–17856. http://dx.doi.org/10.1523/JNEUROSCI.0843-12.2012

Haglund, C.M., J.E. Choe, C.T. Skau, D.R. Kovar, and M.D. Welch. 2010. Rickettsia Sca2 is a bacterial formin-like mediator of actin-based motility. *Nat. Cell Biol.* 12:1057–1063. http://dx.doi.org/10.1038/ncb2109

Husson, C., L. Renault, D. Didry, D. Pantaloni, and M.F. Carlier. 2011. Cordon-Bleu uses WH2 domains as multifunctional dynamizers of actin filament assembly. *Mol. Cell.* 43:464–477. http://dx.doi.org/10.1016/j.molcel.2011.07.010

Kang, H., M.J. Bradley, B.R. McCullough, A. Pierre, E.E. Grintsevich, E. Reisler, and E.M. De La Cruz. 2012. Identification of cation-binding sites on actin that drive polymerization and modulate bending stiffness. *Proc. Natl. Acad. Sci. USA.* 109:16923–16927. http://dx.doi.org/10.1073/pnas.1211078109

Kovar, D.R. 2006. Molecular details of formin-mediated actin assembly. *Curr. Opin. Cell Biol.* 18:11–17. http://dx.doi.org/10.1016/j.ceb.2005.12.011

Kovar, D.R., and T.D. Pollard. 2004. Insertional assembly of actin filament barbed ends in association with formins produces piconewton forces. *Proc. Natl. Acad. Sci. USA.* 101:14725–14730. http://dx.doi.org/10.1073/pnas.0405902101

Kovar, D.R., J.R. Kuhn, A.L. Tichy, and T.D. Pollard. 2003. The fission yeast cytokinesis formin Cdc12p is a barbed end actin filament capping protein gated by profilin. *J. Cell Biol.* 161:875–887. http://dx.doi.org/10.1083/jcb.200211078

Kovar, D.R., E.S. Harris, R. Mahaffy, H.N. Higgs, and T.D. Pollard. 2006. Control of the assembly of ATP- and ADP-actin by formins and profilin. *Cell.* 124:423–435. http://dx.doi.org/10.1016/j.cell.2005.11.038

Kuhn, J.R., and T.D. Pollard. 2005. Real-time measurements of actin filament polymerization by total internal reflection fluorescence microscopy. *Biophys. J.* 88:1387–1402. http://dx.doi.org/10.1529/biophysj.104.047399

Liverman, A.D., H.C. Cheng, J.E. Trosky, D.W. Leung, M.L. Yarbrough, D.L. Burdette, M.K. Rosen, and K. Orth. 2007. Arp2/3-independent assembly of actin by *Vibrio* type III effector VopL. *Proc. Natl. Acad. Sci. USA.* 104:17117–17122. http://dx.doi.org/10.1073/pnas.0703196104

Madasu, Y., C. Suarez, D.J. Kast, D.R. Kovar, and R. Dominguez. 2013. Rickettsia Sca2 has evolved formin-like activity through a different molecular mechanism. *Proc. Natl. Acad. Sci. USA.* 110:E2677–E2686. http://dx.doi.org/10.1073/pnas.1307235110

McCullough, B.R., E.E. Grintsevich, C.K. Chen, H. Kang, A.L. Hutchison, A. Henn, W. Cao, C. Suarez, J.L. Martiel, L. Blanchoin, et al. 2011. Cofilin-linked changes in actin filament flexibility promote severing. *Biophys. J.* 101:151–159. http://dx.doi.org/10.1016/j.bpj.2011.05.049

Montaville, P., A. Jégou, J. Pernier, C. Compper, B. Guichard, B. Mogessie, M. Schuh, G. Romet-Lemonne, and M.F. Carlier. 2014. Spire and Formin 2 synergize and antagonize in regulating actin assembly in meiosis by a ping-pong mechanism. *PLoS Biol.* 12:e1001795. http://dx.doi.org/10.1371/journal.pbio.1001795

Namgoong, S., M. Boczkowska, M.J. Glista, J.D. Winkelman, G. Rebowski, D.R. Kovar, and R. Dominguez. 2011. Mechanism of actin filament nucleation by *Vibrio* VopL and implications for tandem W domain nucleation. *Nat. Struct. Mol. Biol.* 18:1060–1067. http://dx.doi.org/10.1038/nsmb.2109

Neidt, E.M., C.T. Skau, and D.R. Kovar. 2008. The cytokinesis formins from the nematode worm and fission yeast differentially mediate actin filament assembly. *J. Biol. Chem.* 283:23872–23883. http://dx.doi.org/10.1074/jbc.M803734200

Palmgren, S., P.J. Ojala, M.A. Wear, J.A. Cooper, and P. Lappalainen. 2001. Interactions with PIP2, ADP-actin monomers, and capping protein regulate the activity and localization of yeast twinfilin. *J. Cell Biol.* 155:251–260. http://dx.doi.org/10.1083/jcb.200106157

Paunola, E., P.K. Mattila, and P. Lappalainen. 2002. WH2 domain: A small, versatile adapter for actin monomers. *FEBS Lett.* 513:92–97. http://dx.doi.org/10.1016/S0014-5793(01)03242-2

Pernier, J., J. Orban, B.S. Avvaru, A. Jégou, G. Romet-Lemonne, B. Guichard, and M.F. Carlier. 2013. Dimeric WH2 domains in *Vibrio* VopF promote actin filament barbed-end uncapping and assisted elongation. *Nat. Struct. Mol. Biol.* 20:1069–1076. http://dx.doi.org/10.1038/nsmb.2639

Pollard, T.D. 2007. Regulation of actin filament assembly by Arp2/3 complex and formins. *Annu. Rev. Biophys. Biomol. Struct.* 36:451–477. http://dx .doi.org/10.1146/annurev.biophys.35.040405.101936

Pollard, T.D., L. Blanchoin, and R.D. Mullins. 2000. Molecular mechanisms controlling actin filament dynamics in nonmuscle cells. *Annu. Rev. Biophys. Biomol. Struct.* 29:545–576. http://dx.doi.org/10.1146/annurev .biophys.29.1.545

Qualmann, B., and M.M. Kessels. 2009. New players in actin polymerization: WH2-domain-containing actin nucleators. *Trends Cell Biol.* 19:276–285. http://dx.doi.org/10.1016/j.tcb.2009.03.004

Quinlan, M.E., J.E. Heuser, E. Kerkhoff, and R.D. Mullins. 2005. *Drosophila* Spire is an actin nucleation factor. *Nature.* 433:382–388. http://dx.doi.org /10.1038/nature03241

Quinlan, M.E., S. Hilgert, A. Bedrossian, R.D. Mullins, and E. Kerkhoff. 2007. Regulatory interactions between two actin nucleators, Spire and Cappuccino. *J. Cell Biol.* 179:117–128. http://dx.doi.org/10.1083/jcb .200706196

Rasson, A.S., J.S. Bois, D.S. Pham, H. Yoo, and M.E. Quinlan. 2015. Filament assembly by Spire: Key residues and concerted actin binding. *J. Mol. Biol.* 427:824–839. http://dx.doi.org/10.1016/j.jmb.2014.09.002

Reidl, J., and K.E. Klose. 2002. *Vibrio cholerae* and cholera: Out of the water and into the host. *FEMS Microbiol. Rev.* 26:125–139. http://dx.doi.org/10 .1111/j.1574-6976.2002.tb00605.x

Spudich, J.A., and S. Watt. 1971. The regulation of rabbit skeletal muscle contraction. I. Biochemical studies of the interaction of the tropomyosin-troponin complex with actin and the proteolytic fragments of myosin. *J. Biol. Chem.* 246:4866–4871.

Suarez, C., R.T. Carroll, T.A. Burke, J.R. Christensen, A.J. Bestul, J.A. Sees, M.L. James, V. Sirotkin, and D.R. Kovar. 2015. Profilin regulates F-actin network homeostasis by favoring formin over Arp2/3 complex. *Dev. Cell.* 32:43–53. http://dx.doi.org/10.1016/j.devcel.2014.10.027

Tam, V.C., D. Serruto, M. Dziejman, W. Brieher, and J.J. Mekalanos. 2007. A type III secretion system in *Vibrio cholerae* translocates a formin/spire hybrid-like actin nucleator to promote intestinal colonization. *Cell Host Microbe.* 1:95–107. http://dx.doi.org/10.1016/j.chom.2007.03.005

Tam, V.C., M. Suzuki, M. Coughlin, D. Saslowsky, K. Biswas, W.I. Lencer, S.M. Faruque, and J.J. Mekalanos. 2010. Functional analysis of VopF activity required for colonization in *Vibrio cholerae*. *MBio.* 1:e00289-10. http://dx.doi.org/10.1128/mBio.00289-10

Winkelman, J.D., C.G. Bilancia, M. Peifer, and D.R. Kovar. 2014. Ena/VASP Enabled is a highly processive actin polymerase tailored to self-assemble parallel-bundled F-actin networks with Fascin. *Proc. Natl. Acad. Sci. USA.* 111:4121–4126. http://dx.doi.org/10.1073/pnas.1322093111

Wühr, M., R.M. Freeman Jr., M. Presler, M.E. Horb, L. Peshkin, S.P. Gygi, and M.W. Kirschner. 2014. Deep proteomics of the *Xenopus laevis* egg using an mRNA-derived reference database. *Curr. Biol.* 24:1467–1475. http:// dx.doi.org/10.1016/j.cub.2014.05.044

Yu, B., H.C. Cheng, C.A. Brautigam, D.R. Tomchick, and M.K. Rosen. 2011. Mechanism of actin filament nucleation by the bacterial effector VopL. *Nat. Struct. Mol. Biol.* 18:1068–1074. http://dx.doi.org/10.1038/nsmb.2110

Zahm, J.A., S.B. Padrick, Z. Chen, C.W. Pak, A.A. Yunus, L. Henry, D.R. Tomchick, Z. Chen, and M.K. Rosen. 2013. The bacterial effector VopL organizes actin into filament-like structures. *Cell.* 155:423–434. http://dx.doi.org/10.1016/j.cell.2013.09.019

Zimmermann, D., A.N. Morganthaler, D.R. Kovar, and C. Suarez. 2016. In vitro biochemical characterization of cytokinesis actin-binding proteins. *Methods Mol. Biol.* 1369:151–179. http://dx.doi.org/10.1007/978-1-4939 -3145-3_12